ANNALI DI GEOFISICA, VOL. XXXIX, N. 5, October 1996

A steady-state *F*-region model and its use for satellite data analysis

Stanimir M. Stankov
Geophysical Institute, Bulgarian Academy of Sciences, Sofia, Bulgaria

Abstract
A steady-state mathematical model of the Earth's upper ionosphere and plasmasphere is presented. In the model the equations of continuity, momentum, and energy balance for O^+, H^+, and He^+ ions are solved numerically along dipole magnetic field lines. As an extension of the model, a searching method is developed for determination of the boundary values in a self-consistent manner. Model results are compared with Atmosphere Explorer satellite measurements.

Key words *mathematical modelling – searching method – comparison with satellite measurements*

1. Introduction

The purpose of this paper is to present a theoretical model developed for simulating the multi-component thermal plasma processes in the Earth's upper ionosphere at low and middle latitudes. The model also aims at the analysis and extensive use of satellite *in-situ* measurements for both theoretical and empirical purposes. These objectives determine its basic features which make the model different from other existing ones, and also justify its development.

The model focusses on the ion composition in the *F*-region and the plasmasphere, and calculates the concentrations of H^+, O^+, He^+ ions, their diffusion velocities, the ion and electron temperatures. Standard hydrodynamics equations are solved along a chosen magnetic field line, thus facilitating the simulation of the transport processes that prevail in the regions of interest.

According to generality of the physical approach, the existing theoretical models can be classified into several categories – from the most general, (almost) self-consistent global models (Roble *et al.*, 1988; Namgaladze *et al.*, 1990), to the specially formulated, investigating specific phenomena, models (Förster and Jakowski, 1988; Hagan *et al.*, 1990). From this aspect, the present model is between these two extremes, but stands closer to the latter. The model is not self-consistent and uses the neutral atmosphere, temperatures, etc. from outside. The strong connection with particular empirical models is deliberately avoided, having in mind a flexibility in the way of specifying input parameters. Values are required in only one point which is arbitrarily chosen on the field line; the distribution is obtained by using formulae. This approach is very convenient when dealing with satellite data – quite often the trajectory does not offer altitude distribution of the measurements.

Using a steady-state mathematical model of the ionospheric *F*-region is reasonable in many

Mailing address: Dr. Stanimir M. Stankov, Geophysical Institute, Bulgarian Academy of Sciences, Acad. G. Bonchev Street, Block 3, Sofia 1113, Bulgaria; e-mail: ionos@bgearn.acad.bg

cases. *First*, during most of the day, the ion-density distribution around hmF_2 is in quasi-equilibrium; this condition is settled in a time of order 10^3 s during the day and 10^4 s during the night (Rishbeth, 1985). In a state of quasi-equilibrium the magnitude of the time derivative $\partial n/\partial t$ in the continuity equation is much less than the magnitude of any other term: production, loss, or transport. The time derivative is significant only during sunrise and sunset periods, or during periods of strong disturbances. *Second*, the time scale of the most ionospheric processes is generally much greater than the time necessary for a satellite to cross the region where the model gives adequate description of these processes. In this case, the satellite measurements present a snapshot of the ionosphere, and a steady-state model may use these measurements adequately. *Third*, the numerical solution of the differential equations composing a steady-state model is usually easier.

Theoretical modelling traditionally faces problems when specifying boundary values for the differential equations that are used. At the lower boundary (at the *F*-region base) the production and loss processes dominate over the transport ones and the ion densities are given as solutions of the respective continuity equations without the divergence term. Since heat production and heat transfer are the most important mechanisms at lower altitudes, the boundary electron and ion temperatures are given as solutions of the energy equations excluding the convection terms. There are two standard ways of solving the poblems with the upper-boundary conditions. The *first* one (Stubbe, 1970; Strobel and McElroy, 1970) is to specify the flux, $\boldsymbol{n}_i\boldsymbol{v}_i$, at some exobase height where diffusive equilibrium prevails. The flux is usually obtained after integrating the continuity equation from the upper boundary to infinity. For the energy equations, the temperature gradients are used as boundary values, usually adopted from measurements. Shortcomings follow from uncertainties in the production rates and the temperatures. Also, the plasma flux at the top of the ionosphere (so called escape flux) is difficult to estimate; there is no reliable model of this flux and it is either omitted or set to some plausible value. The *second* way (Young *et al.*, 1980; Bailey and Sellek, 1990) is to eliminate the upper boundary by solving the equations along the entire field line – from one point (at the *F*-region base) in one hemisphere to the conjugate point in the opposite hemisphere. Thus, the boundary conditions are of the same type – as for the lower boundary – and the photochemical-equilibrium conditions are used again. While avoiding the problems associated with the upper boundary, this method faces other difficulties arising from the interhemispheric coupling and the validity for closed field lines only. Also, sophisticated numerical treatment of the equation is needed, including a series of coordinate transformations (Kendall, 1962; Sterling *et al.*, 1969; Stankov, 1990), to obtain accurate numerical solution within a reasonable computing time. There are also other methods concerning the upper boundary. Assuming symmetry of ionospheric parameters with respect to the equatorial plane, boundary conditions might be constructed at the equator-crossing point (Baxter, 1967). Another method (Waldman, 1973) uses boundary conditions that are not associated with any particular point of the solution interval; the price is – restriction to certain type of measurements, the most reliable of which is the total electron content. A completely different approach is constituted by the iterative procedures based on the so called «shooting method» – knowing the desired value at the far end, to obtain the value at the close end. Starting with a finite value at the upper boundary, the differential equation is solved after a series of systematic trials to obtain certain quantities at a low altitude – electron density approaching zero, ion/electron density derived from photochemical equilibrium conditions (Moffett and Murphy, 1973), etc. In the model presented in this paper the difficulties associated with the specification of the upper-boundary conditions are overcome by decoupling the continuity and momentum equations and transforming them into a set of first-order differential equations. The Cauchy problem is stated; thus, boundary (initial) values are required at the lower boundary only. This values might be obtained either by fol-

lowing the popular way of using the photochemical equilibrium conditions, or by the searching method offered in section 3. Considering the objectives of creating the model, a novel method for determination of lower-boundary conditions is developed. Based on physical consideration, measurements, empirical and theoretical modelling results, the method employs a searching procedure for locating the most appropriate boundary values for specific temporal and spatial conditions.

In section 4, model calculations for low and high solar activity are given. The results for low solar activity are compared with satellite measurements. In the last section 5, some model applications are discussed along with a non-traditional use of satellite *in situ* measurements. The satellite measurement data may be very useful when solving certain problems, *e.g.*, creating/improving empirical models of some ionospheric quantities, creating/testing regional maps of some characteristics like f_0F_2, etc.

2. Mathematical model

The model is based on the mass, momentum, and energy conservation equations as formulated in Banks and Kockarts (1973) and Kutiev (1986), modified to reflect the assumptions made in the introduction.

The model geometry employs the concept of a plasma tube having the profile of the magnetic field line passing at a given moment through this tube. A centred-dipole magnetic field is assumed. Thus, the Earth's magnetic induction field $\boldsymbol{B}$ is given by

$$\boldsymbol{B} = 0.311 \frac{r_e^3}{r^3} \left(1 + 3 \sin^2 \theta\right)^{0.5}$$

and the equation of a field line is

$$r = r_{eq} \cos^2 \theta$$

where r radial distance from the Earth's centre, r_e Earth's radius, r_{eq} equatorial radial distance of the magnetic field line, θ dipole latitude.

2.1. *Model's set of equations*

The continuity equation, written for the $i^{\text{-th}}$ ion (i = 1(H^+), 2(O^+), 3(He^+)), and parallel to the magnetic field line, is

$$\boldsymbol{B} \frac{\partial}{\partial s} \left(\frac{1}{\boldsymbol{B}} n_i \boldsymbol{v}_i \right) = P_i - L_i$$

where n_i ion concentration, $\boldsymbol{v}_i$ ion field aligned velocity, P_i ion production rate, L_i ion loss rate, $\boldsymbol{B}$ magnetic induction, s arc length along magnetic field line.

The total ion production and loss rates, P_i and L_i, are calculated by

$$P_i = \alpha_{i,\,ph}\, n_i + \sum_j \alpha_{ij}\, \eta_j, \qquad L_i = \sum_j \beta_{ij}\, n_i$$

where n_i ion concentration, η_j concentration of $j^{\text{-th}}$ neutral species, $\alpha_{i,\,ph}$ photoionization rate coefficient for $i^{\text{-th}}$ ion, α_{ij}, β_{ij} chemical reactions' rate coefficients.

The model chemistry is based on production and loss reactions listed in table I. The coefficients α_{ij}, β_{ij} (Bailey and Sellek, 1990) depend on neutral concentrations. Minimum and maximum values of photoionization rate coefficients (for minimum and maximum solar activity) are calculated using the standard photoionization model (Banks and Kockarts, 1973; Hargreaves, 1992), the Mass Spectrometer/Incoherent Scatter (MSIS) model (Hedin *et al.*, 1991), and the 37-band EUV model (Tobishka and Barth, 1990). For a specific solar activity

Table I. Ion production and loss reaction.

Ion	Production	Loss
H^+	Photoionization $O^+ + H \rightarrow H^+ + O$	$H^+ + O \rightarrow O^+ + H$
O^+	Photoionization $H^+ + O \rightarrow O^+ + H$	$O^+ + H \rightarrow O + H^+$ $O^+ + N_2 \rightarrow NO^+ + N$ $O^+ + O_2 \rightarrow O_2^+ + O$
He^+	Photoionization	$He^+ + N_2 \rightarrow He + N_2^+$ $He^+ + O_2 \rightarrow He + O_2^+$

the necessary photoionization coefficients are interpolated.

The ion *momentum* equation can be derived from Boltzmann's equation in hydrodynamic approximation. It takes into account the important forces due to gravity, pressure gradients, electric field, and collisions. Considering the steady-state condition ($\partial v/\partial t = 0$) and ignoring the inertial term ($v\,\partial v/\partial s$) which is not important at low and middle latitudes (Banks and Holzer, 1969), the equation obtains the form

$$g \sin I + \frac{1}{n_i m_i}\frac{\partial p_i}{\partial s} - \frac{1}{m_i} eE + \nu_{in}(v_i - v_w) + \sum_{\substack{j=1 \\ j\neq i}}^{3} \nu_{ij}(v_i - v_j) = 0$$

where c_B Boltzmann's constant, E component of electric field parallel to the magnetic field line, e magnitude of the electron charge, n_i ion concentration, p_i isotropic pressure, m_i ion mass, v_i ion field aligned velocity, v_w neutral wind field aligned velocity ($v_w = v_n \cos I$), v_n horizontal component of v_w, I magnetic inclination, ν_{ij} collision frequency between i and j ion species, $\nu_{ij} = a_{ij}(T_i)n_j$, T_i ion temperature, η_j neutral concentration, T_n neutral temperature, ν_{in} collision frequency between $i^{\text{-th}}$ ion and the neutral species, $\nu_{in} = \sum_{j=1}^{5} b_j(T_j, T_n)\eta_j$, a_{ij}, b_j coefficients (Bailey, 1983).

Assuming the perfect-gas law, the equation is transformed to

$$m_i g \sin I + \frac{c_B T_i}{n_i}\frac{\partial n_i}{\partial s} + c_B(1-\alpha_i)\frac{\partial T_i}{\partial s} - eE + m_i \nu_{in}(v_i - v_w) + \sum_{\substack{j=1 \\ j\neq i}}^{3} m_i \nu_{ij}(v_i - v_j) = 0$$

where α_i denotes the coefficient of thermal diffusion.

Electrons, because of their small mass, are much faster (~ 100 times) than ions. The generated electric field (polarization field) prevents further separation of the opposite charged particles and they all diffuse with comparable velocities (Akasofu and Chapman, 1972). By assuming plasma flux parallel to dipole field lines, the polarization field eE is defined

$$-eE = \frac{c_B T_e}{n_e}\frac{\partial n_e}{\partial s} + c_B \frac{\partial T_e}{\partial s}$$

which is actually an approximation of the momentum equation for the electrons. Replacing eE, the final form of the ion momentum equation is

$$m_i g \sin I + \frac{c_B T_i}{n_i}\frac{\partial n_i}{\partial s} + c_B(1-\alpha_i)\frac{\partial T_i}{\partial s} + \frac{c_B T_e}{n_e}\frac{\partial n_e}{\partial s} + c_B \frac{\partial T_e}{\partial s} + m_i \nu_{in}(v_i - v_w) + \sum_{\substack{j=1 \\ j\neq i}}^{3} m_i \nu_{ij}(v_i - v_j) = 0.$$

Since the thermal conduction takes place mainly along the field lines, the *heat balance* equation for the $i^{\text{-th}}$ ion (after ignoring the total derivative in time), is

$$\frac{\partial}{\partial s}\left(k_i \frac{\partial T_i}{\partial s}\right) = \left(c_B n_i \frac{\partial v_i}{\partial s}\right) T_i - Q_i,$$

$$k_i = 1.2 \times 10^4 \frac{n_i}{n_e} T_i.$$

The generalized ion heating rate, Q_i, combines heating and cooling processes:

$$Q_i = Q_{ie} + \sum_{\substack{j=1 \\ j\neq i}} Q_{ij} + Q_{in}^{el} + Q_{in}^{in}, \qquad i = 1, 2, 3.$$

Included are elastic collisions with: electrons Q_{ie}, other ion species Q_{ij}, neutrals Q_{in}, and inelastic collisions with parent neutrals Q_{in}^{in}. Due to Coulomb interactions, the temperature of the different ion species remains almost same in most of the cases (Rishbeth and Garriott, 1969). For the purpose of this model, the as-

sumption $T_{H^+} = T_{O^+} = T_{He^+} = T_i$ is acceptable. Hence, the equation of the ion temperature can be generalized

$$\frac{\partial^2 T_i}{\partial s^2} = a_i T_i^{-1} \left(\frac{\partial T_i}{\partial s}\right)^2 + a_2 T_i^{-1.5} + a_3 T_i^{-2.5}$$

$$a_1 = -2.5 \qquad a_2 = \frac{c_B}{1.2\times 10^4}\left(\sum_{i=1}^{3} n_i \frac{\partial v_i}{\partial s}\right)$$

$$a_3 = \frac{c_B}{1.2\times 10^4}\left(\sum_{i=1}^{3} Q_i\right).$$

The equation of the electron temperature is

$$\frac{\partial}{\partial s}\left(k_e \frac{\partial T_e}{\partial s}\right) = \left(c_B n_e \frac{\partial v_e}{\partial s}\right) T_e - Q_e,$$

$$k_e = 7.75\times 10^5\, T_e^{2.5}.$$

The electron heating rate includes (Bailey, 1983; Bailey *et al.*, 1986), heating $Q_{ph,\,e}$ by energetic photoelectrons, fine structure excitation of neutral oxygen Q_{en}^{f}, and also rotational Q_{en}^{rot}, vibrational Q_{en}^{vib}, elastic collisions with ion species Q_{ei}, *i.e.*,

$$Q_e = \sum_{i=1}^{3} Q_{ei} + Q_{en}^{rot} + Q_{en}^{vib} + Q_{en}^{f} + Q_{ph,\,e}.$$

Considering the form of the adopted thermal conductivity, k_e, the equation is transformed to

$$\frac{\partial^2 T_e}{\partial s^2} = b_i T_e^{-1} \left(\frac{\partial T_e}{\partial s}\right)^2 + b_2 T_e^{-2.5} + b_3 T_e$$

$$b_1 = -2.5 \qquad b_2 = -\frac{1}{7.75\times 10^5} Q_e$$

$$b_3 = \frac{1}{7.75\times 10^5} c_B n_e \frac{\partial v_e}{\partial s}.$$

In the model there is opportunity for alternative calculation of the ion and electron temperatures (see section 2.2).

2.2. *Model's input parameters*

Aiming at self-consistency by including more and more equations into a model's system is justified if the equation coefficients and boundary values are well known. Otherwise it is reasonable to adopt quantities from measurements/empirical models, thus achieving almost the same results. As it has been said, the model is not self-consistent. The basic model inputs are the quantities related to the neutral atmosphere such as: the concentration of neutral constituents, neutral gas temperature, exospheric temperature, velocity of the neutral wind. Also, an alternative way of calculating the ion and electron temperatures is envisaged. Note that values are required in only one point arbitrarily chosen on the field line. This is very convenient when using satellite measurements because the satellite trajectories do not always provide altitude distribution. If necessary, the computer code allows the input parameters to be included from some empirical model (*e.g.*, MSIS) for the entire interval of integration.

2.2.1. Neutral concentration

Assuming the barometric law distribution, the formula used for calculating the neutral concentration is:

$$\eta_j(h) = \eta_j(h_b)\,\frac{T_n(h_b)}{T_n(h)}\,\exp\left(-\frac{h-h_b}{H_j}\right),$$

$$j = 1\,(\mathrm{H}),\ 2\,(\mathrm{O}),\ 3\,(\mathrm{He}),\ 4\,(\mathrm{N_2}),\ 5\,(\mathrm{O_2})$$

where $\eta_j(h)$ concentration of $j^{\text{-th}}$ neutral species at altitude h, H_j scale height ($= c_B T_j/m_j g$) of the $j^{\text{-th}}$ neutral gas, m_j mass of $j^{\text{-th}}$ neutral species, $T_n(h)$ temperature of the neutral gas at altitude h, h_b base altitude.

It is necessary to set the neutral concentrations at a base height, h_b. The base height may be chosen independently from the starting height h_s (where initial values for the differential equations are given).

2.2.2. Neutral temperature

The temperature of the neutral gas $T_n(h)$ is calculated using the expressions

$$T_n(h) = (a_1 T_{ex} - a_2)(h - h_a) + T_{ex} + a_3 (h_p - h_a)^{0.5} \qquad h \in (150,\ h_a)$$

$$T_n(h) = a_4 (h - h_a)^{0.5} + T_n(h_a) \qquad h \in (h_a,\ h_p)$$

$$T_n(h) = T_{ex} \qquad h \in (h_p,\ +\infty)$$

$$T_n(h_a) \cong T_{ex} - a_3 (h_p - h_a)^{0.5}$$

$$h_a = 200 \text{ km} \qquad a_1 = 8.75 \times 10^{-3} \qquad a_3 = -9.428$$

$$h_p = 0.327 T_{ex} + 27 \qquad a_2 = 1.75 \qquad a_4 = 9.48$$

where T_{ex} means exospheric temperature.

2.2.3. Electron and ion temperatures

For plasma dominated by heat conduction along the field lines, the electron temperature may be calculated by

$$T_e(h) = T_e(h_b) \left\{ 1 + 3.5 (h - h_b) \left[\frac{d}{dh} (\ln T_e) \right]_{h_b} \right\}^{2/7}.$$

This formula is obtained after solving the steady-state heat conduction equation for a fully ionized plasma without considering the local heating/cooling processes.

For calculating the ion temperature, the following expression is used

$$T_i(h) = \frac{\{T_n(h) + \eta(h) [T_e(h)]^{-0.5}\}}{\{1 + \eta(h) [T_e(h)]^{-1.5}\}},$$

$$\eta(h) = 0.1 \times 10^{13} \left(\sum_{j=1}^{5} \eta_j(h) \right)^{-1}.$$

With this expression, the ion temperature is closer to the neutral temperature at low altitudes, but at some altitudes (~ 500 km) it starts approaching the electron temperature.

2.2.4. Thermal diffusion coefficients

The collisions and gradients in the temperatures of the charged particles cause the process of thermal diffusion (Schunk and Walker, 1969; Schunk and Walker, 1970). As a result, the heavier ions are driven towards regions of higher temperature and the light ions towards regions of lower temperature. In this model the O^+ and H^+ are considered major ions, and He^+ minor. The effect of the thermal diffusion on the minor constituents depends on the density ratio of the major ions; thus He^+ ions are driven downwards at low altitudes where O^+ is dominant, and upwards at higher altitudes where H^+ is in abundance. The thermal diffusion is expressed quantitatively (Stubbe, 1973) by coefficients, α_i, in the momentum equations.

2.2.5. Neutral wind

The meridional neutral wind is only considered, with the effect of lowering or raising the ionosphere. During the day, the poleward wind (with velocity generally less than 150 m/s) balances production thus lowering the *F*-layer. During the night, the equatorward wind (less than 300 m/s) helps maintain the *F*-region. At the base height, the horizontal component of the wind velocity is used as a model's input parameter obtained from measurements, simple patterns approximating its diurnal variations, or a reference model (Hedin *et al.*, 1991). Because of viscosity, the altitude variations in the velocity above 200-250 km are small and might be neglected; otherwise the cited model is used.

2.2.6. Inclusion of the electromagnetic ($\boldsymbol{E}\times\boldsymbol{B}$) drift

The effect of the electromagnetic ($\boldsymbol{E}\times\boldsymbol{B}$) drift is included implicitly in the model calculations. The $\boldsymbol{E}\times\boldsymbol{B}$ drift moves a given plasma tube causing compression or expansion of the plasma. If the change in tube's position is known, the changes ΔP and ΔL in production and loss terms respectively, are also known. Then, for the new values P' and L' we may write $P' = P + \Delta P$, $L' = L + \Delta L$. Instead of cal-

culating ΔP and ΔL it is easier to correct the neutral concentrations. The concentrations of the j^{-th} neutral constituent is multiplied by the expression (Koleva and Kutiev, 1987)

$$\aleph = \frac{H_j}{\Delta h}\left\{1 - \exp\left(-\frac{\Delta h}{H_j}\right)\right\}$$

where H_j is the scale height of the j^{-th} neutral gas and Δh is the displacement (in altitude direction) due to the $\boldsymbol{E}\times\boldsymbol{B}$ drift. This assumption is valid when the drift is changing slowly, *i.e.*, not appropriate for sunrise and sunset periods.

2.3. *Numerical solution*

The complete set of the model's equations is given below

$$\frac{\partial n_i}{\partial s} = -\frac{n_i}{c_B T_i}\left(m_i g \sin I + c_B(1-\alpha_i)\frac{\partial T_i}{\partial s} + \right.$$

$$\left. + m_i \nu_{in}(\boldsymbol{v}_i - \boldsymbol{v}_w) + \sum_{\substack{j=1 \\ j\neq i}}^{3} m_i \nu_{ij}(\boldsymbol{v}_i - \boldsymbol{v}_j) - e\boldsymbol{E}\right)$$

$i = 1(H^+),\ 2(O^+)\ 3(He^+)$

$$\frac{\partial \boldsymbol{v}_i}{\partial s} = \frac{1}{n_i}\left(P_i - L_i - \boldsymbol{v}_i\frac{\partial n_i}{\partial s}\right)$$

$i = 1(H^+),\ 2(O^+),\ 3(He^+)$

$$\frac{\partial^2 T_i}{\partial s^2} = a_i T_i^{-1}\left(\frac{\partial T_i}{\partial s}\right)^2 + a_2 T_i^{-1.5} + a_3 T_i^{-2.5}$$

$$\frac{\partial^2 T_e}{\partial s^2} = b_i T_e^{-1}\left(\frac{\partial T_e}{\partial s}\right)^2 + b_2 T_e^{-1.5} + b_3 T_e$$

$$n_e = \sum_i n_i$$

$$e\boldsymbol{E} = -\left(\frac{c_B T_e}{n_e}\frac{\partial n_e}{\partial s} + c_B\frac{\partial T_e}{\partial s}\right).$$

The ordinary differential equations are nonlinear, of first and second order, and are solved numerically along the field line by using predictor-corrector methods (Gear, 1971; Dahlquist and Björck, 1974). The integration starts from a *starting* height, h_s, and continues up to an arbitrary *upper* altitude, h_u. The molecular ions, prevailing at very low altitudes, are not considered, so h_s is usually ~200 km. The solution is obtained in two stages: for altitudes $h\in(h_s, h_j)$ and for altitudes $h\in(h_j, h_u)$. The «joining height», h_j, may vary and is chosen after considering the following. At lower altitudes (near hmF_2) the O^+ ion is the dominant ion and the differential equations are solved for this ion only using the coupled version of the system, *i.e.*, the $e\boldsymbol{E}$ expression placed in the first equation. In this region, the H^+ ion concentration is controlled mainly by the charge exchange reactions between O^+ and H, and between H^+ and O. To a high level of accuracy, the H^+ concentration might be obtained by the well-known formula:

$$n(H^+) = 1.125\frac{\eta(H)}{\eta(O)}\left(\frac{T_n}{T_i}\right)^{0.5} n(O^+)$$

where the constant arises from statistical estimations concerning the exchange reactions. In chemical equilibrium conditions, the He^+ concentration is given approximately by

$$n(He^+) = \frac{I(He)\,\eta(He)}{c_1\,\eta(N_2) + c_2\,\eta(O_2)}$$

where $I(He)\eta(He)$ represents the direct photoionization of the neutral He and c_1, c_2 are rate coefficients. At night the photoionization of He is slight and takes place in the sunlit parts of the plasma tube. At altitudes below ~400 km, the He^+ concentration is extremely low due to the high concentration of N_2 and O_2 and the corresponding loss reactions. This fact could significantly impede a numerical solution of the differential equations in a coupled

system. At higher altitudes the diffusion starts prevailing and these formulas become invalid. Also, the second stage of integration should start sufficiently below the O^+-H^+ transition height. Summarizing, the joining height h_j should be in the optimal range 500-600 km.

At each step the differential equations are solved consecutively in the following order: continuity, momentum, electron temperature, ion temperature. The solution procedure is repeated iteratively until convergence of n_e (for altitudes below h_j) and of $\boldsymbol{eE}$ (for altitudes above h_j) is achieved.

It is necessary to specify the initial values $n_s(O^+)$, $\boldsymbol{v}_s(O^+)$, $T_{i,s}$, $T_{e,s}$, $\left(\frac{\partial T_i}{\partial s}\right)_s$, $\left(\frac{\partial T_e}{\partial s}\right)_s$ at the starting height, h_s. Following the standard procedure, the value $n_s(O^+)$ is obtained from the chemical equilibrium condition $P_i = L_i$. During the night $n_s(O^+)$ is calculated after assuming that, along the field line, the O^+ concentration is proportional to the corresponding gradient of the loss coefficient (Murphy *et al.*, 1980). The ion velocity value at altitudes around 200 km is not important and is set equal to zero: after some steps along the field line, the real velocity is achieved.

In general, the effects of any finite velocity at the lower boundary are attenuated within about a scale height (Lindzen, 1966). Under 250 km the coupling between the ion and neutral constituents is strong enough to keep the ion and neutral temperatures almost equal. Hence, it might be written

$$T_i(h_s) = T_{n,s} \qquad \frac{\partial T_i}{\partial s}(h_s) = \frac{\partial T_{n,s}}{\partial s}.$$

The starting values for the electron temperature are obtained from the commonly used condition $Q_e = 0$.

For the second stage all the initial values may be set using the calculations for the first stage. In the following section an alternative way of obtaining the initial density values is proposed.

3. A searching method for self-consistent determination of the boundary values

The model presented in the previous section is not self-consistent: differential equations for the ion densities, velocities, ion and electron temperatures are only solved. The quantities characterising the neutral atmosphere are adopted as model's inputs. Such treatment raises some problems. *First*, a numerical solution of the model equations strongly depends on the inputs; and these inputs should be precise. In most of the cases empirical models (*e.g.*, MSIS, CIRA) are used and those models are not perfect. *Second*, the strong dependence of the numerical solution on the neutral atmosphere, especially daytime, does not guarantee uniqueness of the solution. The main reason for that is the transport processes. The major physical processes contributing to the plasma transport at low and middle latitudes are (Rishbeth, 1985): thermal expansion and contraction of the atmosphere, plasma diffusion, fluxes into and out of the plasmasphere, electric field causing the electromagnetic drift, and neutral wind. *Third*, it is necessary to set boundary values for the differential equations, which is always difficult to do precisely.

In the steady-state model, ordinary differential equations are solved (Cauchy problem), *i.e.*, only one boundary (initial) value is required. The solution is very sensitive to the initial density value. Model calculations, using seven different initial O^+ density values and keeping all other daytime input parameters constant, are presented in fig. 1a,b. On the upper panel (fig. 1a) the O^+ density profiles are given, and their corresponding velocity profiles are on the bottom panel (fig. 1b). The initial values are very close to each other and are not discernible visually. The figure shows the strong dependence between the density and velocity profiles as well. For example, the curves 2 represent the case of strong upward O^+ flux, while the profiles 7 demonstrate a downward flux. On the one hand, it is obvious that all the model's input parameters (including the initial value) should be correct to obtain reliable results. For instance, profile 1 is obviously «degenerate» (not possible from a physical view-

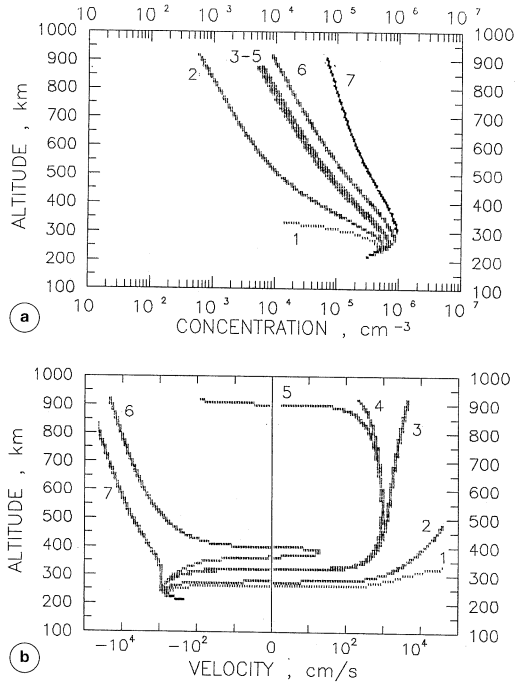

Fig. 1a,b. Dependence of ion profiles on the initial O^+ density, $n_s(O^+)$. a) density profile; b) velocity profile.

point) and its corresponding initial value is very close to the good initial values giving curves 3-5. On the other hand, the demonstrated high sensitivity on the boundary (initial) value, when combined with the necessity of specifying only one boundary value and the freedom of arbitrarily choosing the length of the integration interval, might be regarded as an advantage. The advantage can be successfully used in creating a method for obtaining the initial values and/or conforming model's results to the model's input parameters in order to satisfy the established structural features of the ionosphere. In some cases the solution could be adjusted to existing (satellite/ground-based ionosonde) measurements.

The idea of the developed method is the following. The uncertainty is concentrated into one input parameter: in this case, the density $n_s(O^+)$ at the starting height h_s. By varying the input parameter the model's results are required to satisfy some *a priori* given conditions (of common physical considerations) on certain profile characteristics. *Profile characteristic* is any of the typical features of all ion profiles, for example NmF_2, hmF_2, etc. *Ion profile* is the altitude distribution of density, velocity, or flux. The calculated profiles must be in conformity with the ionospheric structural features and/or measurements. The procedure is divided into two main parts: construction of the O^+ profile for the lower (h_s, h_j) altitude range, and construction of the O^+, H^+, He^+ profiles in the upper (h_j, h_u) altitude range.

First, it is necessary to emphasise some important features of the daytime and nighttime ionosphere. *Daytime*, the ion production and loss depend strongly on the neutral atmosphere composition. Let us consider the flux balance in the ionosphere. On the one side, the dominating photoionization process generates a powerful upward flux that fills the plasmasphere. On the other, given the high concentration of N_2 and O_2 at lower altitudes, the O^+ sink at the base of F_2-region is great. Also, because of the short life of plasma in the F_1-layer and below, it is unlikely that large vertical drifts could exist to bring plasma from below the F_2-region (Rishbeth, 1985). Hence, a downward O^+ flux should come from above. As a result, an altitude should exist – from this altitude above an upward O^+ flux takes place, and from this altitude below – there is another downward O^+ flux. Such a height exists (see fig. 1b) and it is close to the height of the F_2 density peak, hmF_2. *Nighttime*, the situation is different. There is no photoionization and the density distribution is not so strictly coupled with the neutral atmosphere. The F-region is maintained by downward fluxes coming from the plasmasphere. The method will be presented in detail for daytime conditions.

3.1. *Lower part (h_s, h_j)*

Four *basic* controlled characteristics have been chosen: NmF_2 (the maximal electron concentration), hmF_2 (the altitude of the maximal

concentration), h_{ch} (the altitude where the plasma flux changes its direction), v_c (O^+ velocity at a given control height h_c). There is another, implicitly controlled characteristic – the plasma flux. However, preference to its components – concentration and velocity is given. Following the idea of the method, the model results have been analysed after varying the initial value $n_s(O^+)$. The influence of the initial O^+ concentration on the behaviour of the controlled characteristics is demonstrated in fig. 2a-d for summer daytime conditions during low solar activity. The characteristics are considered functions of one variable, $n_s(O^+)$. There are two important test results. *First*, all functions are continuous and monotonous in the whole interval of possible initial values. The only exception is the altitude h_{ch}: it is also continuous and monotonous but up to a specific interruption point. For initial values greater than this point, model calculations give negative O^+ velocity for the entire altitude range which is impossible in the daytime according to the notes above. *Second*, significant changes in the characteristics' behaviour occur only in a narrow initial-value interval. In fig. 2a-d it is approximately $(1.65 \times 10^5,\ 1.75 \times 10^5\ \mathrm{cm}^{-3})$. From this aspect, the most sensitive characteristics are v_c and h_{ch}. Considering the theoretical notes above, broad limitations are set for each of the controlled characteristics, embracing their possible variations for different spatial temporal and geophysical conditions. For instance, the existence of two oppositely directed fluxes means that at the altitude h_{ch} the O^+ velocity changes its direction. Hence, in the model results, the altitude must exist and should be near (say ± 20 km) the altitude hmF_2. As regards the upward flux, its existence means that at a control level h_c (well above hmF_2) the diffusion velocity v_c should have a positive value. A natural limitation for low and middle latitude is this velocity to be subsonic (Banks and Kockarts, 1973).

The continuity and monotony are very useful: they guarantee convertibility of the functions. In other words, for any interval $\boldsymbol{r}$ of function values, it is possible to find the corresponding interval $\boldsymbol{i}$ of variable values; any element of $\boldsymbol{i}$ gives a function value that is in $\boldsymbol{r}$. Let us set

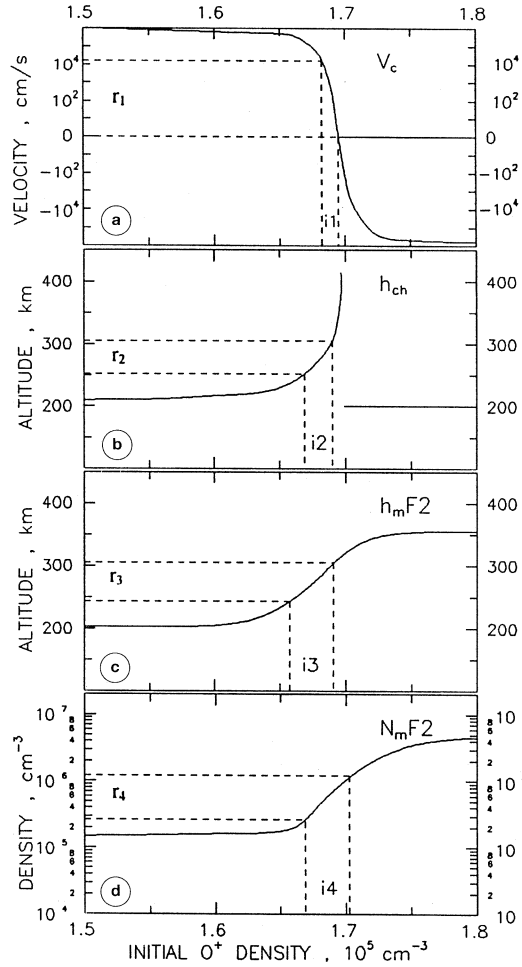

Fig. 2a-d. Dependence of the contolled profile characteristics on the initial O^+ density, $n_s(O^+)$. a) v_c velocity at the control height, h_c; b) h_{ch} altitude where velocity changes its direction; c) hmF_2 height of the peak density; d) NmF_2 the peak density.

example limitations on the controlled characteristics: $NmF_2 \in (2.8 \times 10^5,\ 1.2 \times 10^6\ \mathrm{cm}^{-3})$, $hmF_2 \in (255,\ 300$ km), $h_{ch} \in (245,\ 310$ km), $v_c(h_c = 900\ \mathrm{km}) \in (0,\ 10^4$ cm/s). These limitations are appropriate for the conditions used in the model test presented in fig. 2a-d. If arranging the limitations on v_c, h_{ch}, hmF_2, NmF_2 as intervals $\boldsymbol{r}_1$, $\boldsymbol{r}_2$, $\boldsymbol{r}_3$, $\boldsymbol{r}_4$ one could find the corresponding initial-

value intervals $\boldsymbol{i}_1$, $\boldsymbol{i}_2$, $\boldsymbol{i}_3$, $\boldsymbol{i}_4$. Obviously, the intersection $\boldsymbol{i}^*$ of $\boldsymbol{i}_1$, $\boldsymbol{i}_2$, $\boldsymbol{i}_3$, and $\boldsymbol{i}_4$ consists of elements $n_s(O^+)^*$, called «*acceptable*»; for these acceptable elements the model gives ion profiles in conformity with all the requirements.

Numerous model tests have been carried out for different model's input parameters. The basic results can be sorted into two categories. First, the controlled characteristics demonstrate the same type of behaviour as shown in fig. 2a-d. Second, the acceptable interval $\boldsymbol{i}^*$ is always narrow. For the case presented in fig. 2a-d, the $\boldsymbol{i}^*$ interval is $(1.67939 \times 10^5, 1.67955 \times 10^5$ cm$^{-3})$. All density profiles, calculated with the initial values within $\boldsymbol{i}^*$, are extremely close to each other and are practically regarded as only one profile.

The procedure for finding the *acceptable* interval is iterative and starts with an arbitrary initial value. The values of the four chosen characteristics are checked and, considering fig. 2a-d, a new initial value is determined. After calculating the new profiles, the controlled characteristics are analysed again, and a new initial value is chosen, etc. The procedure continues until one acceptable value $n_s(O^+)^*$ is obtained. If high accuracy is sought, the acceptable interval is extended by small steps aside of $n_s(O^+)^*$. Once determining the O^+ profile, the H^+ and He^+ density profiles might be calculated using the chemical-equilibrium formulae.

3.2. *Upper part (h_j, h_u)*

The method for constructing the O^+, H^+, and He^+ profiles for the upper altitude range is slightly different due to the different physical conditions near the ionosphere-plasmasphere coupling region. During the day there is an upward plasma flux filling the plasmasphere. The O^+ flux, generated in the *F*-region, is transformed into an upward H^+ flux thanks to the charge-exchange reaction $O^+ + H \rightarrow O + H^+$. Little is known about the He^+ ion flux. This flux is smaller in magnitude than the H^+ flux and shows a latitudinal behaviour due to the near diffusive equilibrium at the equator and the dynamic equilibrium at the high-latitude regions (Chandler and Chappell, 1986).

The controlled characteristics for the upper integration interval are the densities $n_{cc}(.)$ and velocities $\boldsymbol{v}_{cc}(.)$ of the O^+, H^+, He^+ ions at a control height h_{cc}, and the O^+-H^+ transition level (the altitude where the O^+ and H^+ ion densities are equal). It is also possible to set some conditions on the behaviour of the chosen characteristics. The velocities of H^+ and He^+ should be positive at the control height h_{cc} (well above the transition levels). Another restriction is the tendency of these velocities to remain subsonic. Moreover, there should be a height where the H^+ flux from downward (negative velocity) becomes upward (positive velocity). Because the exchange reaction $O^+ + H \rightarrow O + H^+$ is very fast, it is logical to conclude that the change in velocity direction takes place at altitudes near the ion transition level. The transition level demonstrates pronounced spatial and temporal variations and a reference empirical model (Kutiev *et al.*, 1994) is used to set limitations on the level.

The searching procedure is iterative again. The model is started from h_j and the equations are solved up to h_u. The model may be started with the already calculated (at the h_j altitude level) values $n_j(O^+)$, $n_j(H^+)$, and $n_j(He^+)$ but the results might be different from the real ones because of imperfection of the H^+ and He^+ chemical-equilibrium formulae used in the lower integration part (Koleva and Kutiev, 1990). Considering the initial value $n_{ss}(O^+)$ acceptable, *i.e.*, assuming $n_{ss}(O^+)^* \equiv n_j(O^+)$, it is necessary to find the acceptable $n_{ss}(H^+)^*$ and $n_{ss}(He^+)^*$. If $n_{ss}(He^+)$ is fixed and $n_{ss}(H^+)$ is being varied, the behaviour of $\boldsymbol{v}_{cc}(H^+)$ and $h_{ch}(H^+)$ is described with monotonous and continuous functions. The situation is similar for $\boldsymbol{v}_{cc}(He^+)$ and $h_{ch}(He^+)$ if $n_{ss}(H^+)$ is fixed. Thus, starting with initial values calculated in the lower part, the profile characteristics are controlled after each iteration until the acceptable H^+ density is determined. After that the He^+ density is associated in a similar manner.

The searching method was presented for daytime conditions. During the night the method is essentially the same. However, it is necessary to take into account the basic features of the nighttime ionosphere, especially the flux directions. Also, the nighttime *F*-layer

is higher than the daytime one, and the small concentrations of O^+ at the *F*-region base may impede the calculations. A possible way of avoiding this problem is to raise the starting height h_s with 10-20 km.

A part of the method is the set of limitations on the controlled profile characteristics. The set embraces the *possible* variations due to local time, latitude, season, and solar activity. Different sources, both theoretical and empirical, were consulted when creating this set. It is being further developed by using new, mainly satellite, measurement data. The variations in the *F*-region electron density, NmF_2, can be reliably obtained by the ground-based ionosonde measurements. For low solar activity the results of the SUNDIAL-86 campaign were used (Szuszczewicz *et al.*, 1988; Sica *et al.*, 1990). The peak density is raised during high solar activity – linear dependencies on the $F_{10.7}$ index are adopted. The height, hmF_2, of the peak is difficult to determine from measurements. One way is to retrieve it from ionograms (Dudeney, 1983). Here, averaged daily cycles of NmF_2 versus hmF_2 were considered (Rishbeth and Edwards, 1989). Data from *Atmosphere Explorer* and *Dynamics Explorer* satellites were also used to improve the set concerning NmF_2 and hmF_2. The height h_{ch} is assumed to be near the altitude hmF_2, so the limitations on the height h_{ch} are bound to the limitations on hmF_2. The basic restrictions imposed on the ion fluxes concern: i) their directions and ii) their subsonic feature. Although there is a theoretical possibility of existing supersonic flows in the plasmasphere (*e.g.*, at extremely low temperatures), it is unlikely to happen (Rishbeth *et al.*, 1978; Murphy and Moffett, 1978; Murphy and Naghmoosh, 1979). The ion velocities at the control height are very sensitive when varying the initial value near the acceptable interval (see fig. 2a); the magnitude falls from supersonic to zero values within very small changes in the initial density. Considering this sensitivity, the only (at this stage) limitation concerning the velocities is the ion velocities to remain subsonic at all times and altitudes. The fluxes are controlled implicitly and limiting values of H^+ and He^+ flows are referenced (Raitt *et al.*, 1978; Naghmoosh and Murphy, 1983; Richards and Torr, 1985). The occurrences of light-ion counterstreaming needs further investigation as it might be significant under certain conditions (Naghmoosh and Murphy, 1983; Chandler and Chappell, 1986; Bailey and Sellek, 1992). It is important to note that the limitation intervals are broad and should be regarded as tools used by the hunting procedure to approach the acceptable interval much faster. For precise determination of the acceptable i^* interval, it is the *model's intrinsic features* and the *combined effect* of the limitations that is relied on. Otherwise, the integrity of the model would be jeopardized.

4. Results

By using the model and the searching method described above, the O^+, H^+, and He^+ density profiles were calculated along a given field line, $L = 1.75$ for low (fig. 3) and high (fig. 4) solar activity. Calculations for nighttime and daytime conditions during all seasons are presented. The neutral atmosphere was taken from MSIS, corrected when possible with the satellite measurements. All temperatures were given as model's input parameters. In the figures the modelled O^+ densities are represented with solid lines, the H^+ densities – with dotted lines, and He^+ with dashed lines. The left side of the figures corresponds to the nighttime conditions and the right side to the daytime conditions. The summer profiles are plotted in the top panels, the equinox profiles are in the middle panels, and the winter profiles in the bottom ones.

4.1. *Low solar activity: comparison between model results and measurement data from the* Atmosphere Explorer *satellite*

The comparison is limited for low solar activity conditions only. For the purpose, the model calculations were compared with measurements from the *Atmosphere Explorer* – C (AE-C) satellite is used. The time span of data is November 1973 – February 1975 and the altitude range is 150-1300 km.

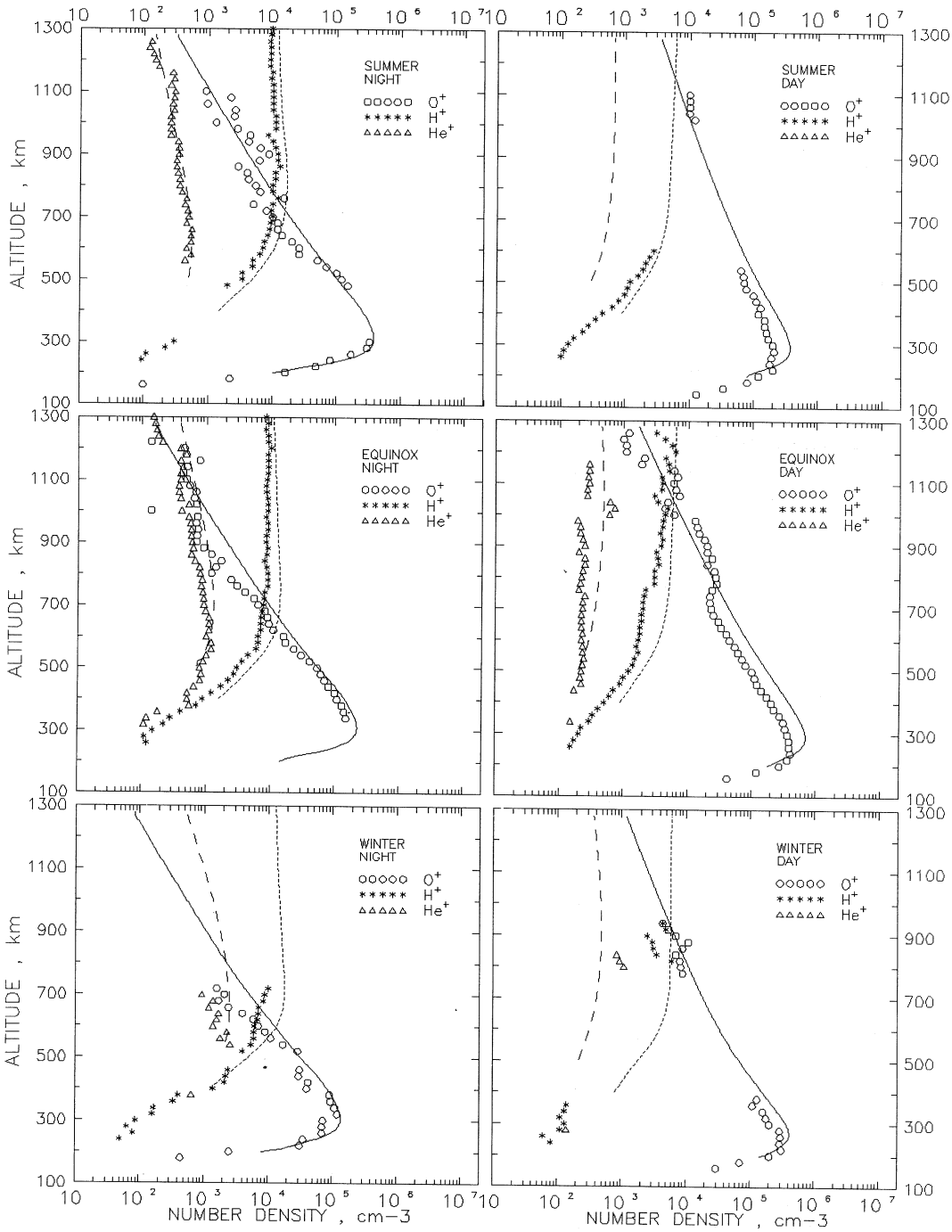

Fig. 3. Model results: low solar activity. Comparison with *Atmosphere Explorer-C* measurements.

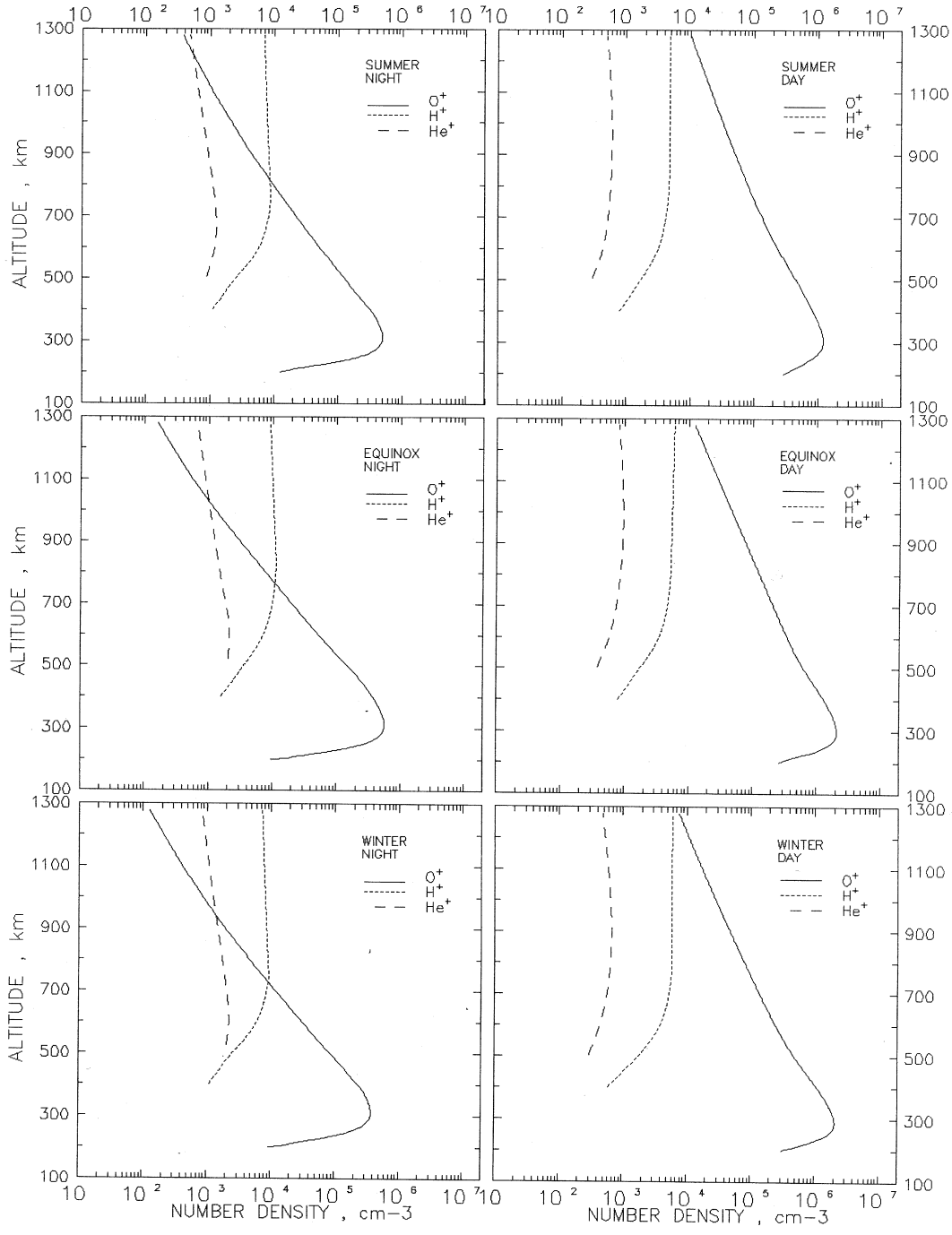

Fig. 4. Model results: high solar activity.

4.1.1. Data base

Ion density data were measured by a Bennet radio frequency mass spectrometer (BIMS) on the AE-C. The data were binned for invariant latitude, local time and season ranges. The latitude range chosen to represent the field line was 35-45° North. An exception was the nighttime profiles during summer where data from the Southern hemisphere were added. For the noon study, the local time of the measurements was restricted to 9:00-15:00 LT and for midnight to 21:00-03:00 LT windows. The seasons were defined as 90 day periods centred on the solstices and equinoxes. No separation was made between the vernal and autumn equinoxes. The winter data were collected from both the first and the second winter. Each symbol (0 for O^+, * for H^+, Δ for He^+) in fig. 3 represents the data averaged over 20 km in altitude.

Figure 3 shows the expected strong local-time and seasonal variations in the ion densities. During all seasons the noon O^+ densities were higher than the midnight densities. The difference varied with altitude and was greater at upper altitudes.

On the contrary, the light-ion densities were generally greater during the night than during the day. The seasonal variation in the O^+ density was small with the equinox values higher than the summer and winter ones. Above the peak density, the summer O^+ density was higher than the equinox and winter densities.

During the night, the summer H^+ density was almost equal to equinox H^+ density at all latitudes and slightly lower than the winter density up to 800 km.

During the day, the summer and winter He^+ density measurements were sparse and greatly scattered, giving not enough information for the seasonal variation. But the nighttime measurements revealed strong seasonal variations mainly below 1000 km. At 600 km, the equinox densities were almost twice the size of those measured during the equinox. The winter He^+ densities were the highest, with a maximum near the O^+-H^+ transition level (~ 600 km).

4.1.2. Model and data comparison

The model was run for summer (day of year 174), equinoxes (days of year 81 and 265) and winter (day of year 356). Model calculations were obtained for each hour in the ranges: 9:00 to 15:00 LT and 21:00 to 3:00 LT. The results were averaged to represent the noon and midnight conditions respectively. At the base height, the neutral densities were adopted from MSIS but the O, He, N_2 densities corrected with satellite measurements through the Neutral Atmosphere Composition Experiment (NACE) when available. The electron temperature and its gradient were taken from the averaged measurements. The solar activity during the mission was low, with the F 10.7 index varying between 70 and 120. An average of F 10.7 = 90 was used and quiet geomagnetic conditions, $Ap = 10$. The initial values of O^+ at h_s and the H^+ and He^+ at h_j were obtained by the searching procedure.

In general, the diurnal and seasonal variations in the ion densities are well reproduced by the model. However, there is a tendency to overestimate the O^+ density for altitudes below 700 km, which is probably due to higher temperatures at the base height h_b (one temperature is used for all local times). The maximum excursions (although within the mean error) from the data is observed for equinox and summer during the day. The electron temperature at h_b was slightly reduced to help matching the modelled nighttime O^+ density (He^+ respectively) to the measured ones.

The upper part of the ion profiles were obtained after starting the model at h_j (varying between 450 and 550 km). At these heights, the formulae (for the photochemical equilibrium) gave higher values for the light-ion densities than the values obtained through the searching procedure. The latter ones are closer to the mean measurement values. There are not enough daytime He^+ data in winter and summer but the equinox panel shows that the model densities are close to the measured ones, slightly higher at greater altitudes. Higher modelled He^+ values were obtained during nighttime as well, especially during equinox and winter. There are peaks in the modelled

densities which were higher than the observed ones for equinox and winter. The modelled H^+ density tended to be higher than the measured one. While the overestimation at lower altitudes may be attributed to the higher O^+ densities, the high H^+ values at greater altitudes suggests also uncertainty in the neutral H values.

4.2. *High solar activity*

The calculations for high solar activity were carried out in a manner similar to that described above. The neutral densities were taken from MSIS again, and the ion and electron temperatures – from IRI. Figure 4 shows the nighttime and daytime ion concentrations as modelled for each season.

A comparison between the corresponding panels of fig. 3 and fig. 4 shows that O^+ and He^+ concentrations were higher at solar maximum. The H^+ concentrations were slightly lower during solar maximum, this being more pronounced during the night. Above the O^+-H^+ transition level, the H^+ ion was the dominant ion at all times. There was no indication that He^+ may dominate. A significant increase in He concentration and the photoionization rate was needed to model the winter He^+ bulge. Ignoring the averaging process in respect to local time, the results suggest uncertainty in the mentioned rate and concentration.

5. Discussion

A steady-state mathematical model of the upper ionosphere has been presented. The model calculates values of the O^+, H^+ and He^+ ion concentrations, velocities, the ion and electron temperatures along a given magnetic field line. The searching method (section 3) determined the initial (boundary) values in a self-consistent manner. Model test results have been compared with Atmosphere Explorer satellite measurements. Using input parameters from the measurements, the results of comparison demonstrate a good agreement between the measured and modelled composition.

However, using all input parameters from the satellite measurements was not always possible: quite often the neutral atmosphere was taken from a reference model which may offer values not consistent with the measurements. The searching method also offered a convenient way of artificial adjustment of the ion profiles to the measurements. For this purpose, it was necessary to define a very short limitation interval (taken from the measurement). Usually, the controlled characteristic, treated in this way, was an ion/electron concentration at a certain (control) height where a satellite measurement is available.

Two major applications of the model are discussed below.

5.1. *Ionospheric mapping*

Special attention is drawn to creating geographic maps of the critical frequency f_0F_2. The traditional ways of mapping this parameter use (global) theoretical models of the electron concentration and/or the interpolation techniques based on ground-based (ionosonde) measurements. In the first case, the theoretical results may differ from the real situation and it is difficult to use measurements for correcting purposes. In the second case, difficulties arise in the regions where the ionosondes are not enough to guarantee reliability of the interpolation. Satellite measurements may be utilized in creating/testing maps of f_0F_2. When topside sounders are available on board, the method is straightforward. The problem is how to utilize *in situ* measurements (neutral/ion/electron densities, temperatures, etc.). It requires a different approach, the essential part of which is the use of a theoretical model to recover an ion density profile from the satellite measurements. The profile would give NmF_2, and the corresponding f_0F_2 is easily calculated. From this aspect, the presented steady-state model is very useful when applying such «tracing method». A distinction is made between the monthly-median mapping (representative for the ionosphere in a given hour of day during a whole month) and the instantaneous mapping (valid for a given hour on a specified day).

For the monthly-median mapping, the satellite density measurements are extracted over a region with negligible differences in f_0F_2 (usually 5° in longitude and 2.5° in latitude) and within a given hour of day during the whole month. The theoretical model is then used to calculate a density profile closely matching the measurements. The modelled f_0F_2 is accepted as a monthly median for the region. The method allows existing ground-based measurements to be utilized for calibrating. The densities are traced down to a fixed level (above the height of the peak density) and the «plasma frequency» is then calculated. In the regions with available ionosonde measurements, the modelled f_0F_2 is divided to the measured f_0F_2. The average ratio is then used to multiply the plasma frequencies in the regions where no ionosonde measurements exist. A modified version of this method was used with AE-C data over Europe (Kutiev and Stankov, 1995).

Given the high variability of the upper ionosphere from day to day, it is not easy to apply the tracing method for the purposes of instantaneous mapping. The basic difficulties arise from the uncertainties in the model's input parameters and the limited satellite data. The measurements are reliable only along the trajectory and the method is more reliable when using additional information, *e.g.*, from an ionosonde along the trajectory. Then, at the point of the ionosonde, two critical frequencies are obtained – modelled ($f_0F_{2\ \mathrm{mod}}$) and measured ($f_0F_{2\ \mathrm{sond}}$). If a difference exists, the uncertainty is transferred to the neutral densities $n(O)$ and $n(N_2)$ (the O^+ production rate depends on $n(O)$, and the loss rate – on $n(N_2)$), and the plasma temperature, Tp. When varying the ratio $n(O)/n(N_2)$ and Tp, the slope of the density profile above the peak also varies, thus affecting hmF_2 and NmF_2. After calibrating $f_0F_{2\ \mathrm{mod}}$ to $f_0F_{2\ \mathrm{sond}}$, the obtained ratio between the new and the original $n(O)/n(N_2)$ and Tp is used for correcting purposes in the remaining part of the trajectory. The method gave satisfactory results when used with Dynamics Explorer data for the region of Europe (Kutiev and Stankov, 1995).

5.2. *Improving empirical models*

The ionosphere is strongly coupled to the neutral atmosphere through photochemical and dynamic interactions. To reliably understand the complicated nature of the ionospheric phenomena, the reference model, providing input parameters, should be reliable in such a way that the measured ionospheric quantities should be reproduced by theory through the theoretical model. Hence, it is necessary sometimes to adjust some input parameters carefully to obtain the above mentioned agreement. The presented model can be a useful working instrument that could involve the satellite measurements. Another aspect is the agreement between two reference models of different nature, *e.g.*, the MSIS and IRI (International Reference Ionosphere) models.

The mathematical model calculates the densities of the important ion species in the upper ionosphere, *i.e.*, O^+, H^+, and He^+ and can be used to improve the ion composition part of existing empirical models. For example, the most reliable model to date, the IRI, gives a constant $n(H^+)/n(He^+)$ ratio. This is not confirmed by the measurements and the model results (figs. 3 and 4). The $n(H^+)/n(He^+)$ varies with altitude and it is significant under certain conditions. The recent satellite measurement data are still not tapped for use in IRI (Bilitza *et al.*, 1993), and this ratio deserves investigation.

Acknowledgements

I thank Prof. Ivan Kutiev for the useful discussions. Thanks are also due to Mr. Peter Bradley and the referees for then comments on the manuscript.

The work was supported by Bulgarian National Scientific Research Foundation under grant NZ14/91. The satellite measurement data were provided by the National Space Science Data Center through the World Data Center A for Rockets and Satellites, Goddard Space Flight Center.

REFERENCES

AKASOFU, S.I. and S. CHAPMAN (1972): *Solar-Terrestrial Physics* (Clarendon Press, Oxford, England).

BAILEY, G.J. (1983): The effect of a meridional E×B Drift on the thermal plasma at $L = 1.4$, *Planet. Space Sci.*, **31** (4), 389-409.

BAILEY, G.J. and R. SELLEK (1990): A mathematical model of the Earth's plasmasphere and its application in a study of He^+ at $L = 3$, *Annales Geophysicae*, **8** (3), 171-190.

BAILEY, G.J. and R. SELLEK (1992): Field-aligned flows of H^+ and He^+ in the mid-latitude topside ionosphere at solar maximum, *Planet. Space Sci.*, **40** (6), 751-762.

BAILEY, G.J., R.J. MOFFETT, P.A. SIMMONS and R.J. FOOTIT (1986): A modelling study of the post-sunset formation of plasma temperature troughs in the equatorial topside ionosphere, *Annales Geophisicae*, **4** (A2), 113-130.

BANKS, P.M. and T.E. HOLZER (1969): Features of plasma transport in the upper atmosphere, *J. Geophys. Res.*, **74** (26), 6304-6316.

BANKS, P.M. and G. KOCKARTS (1973): *Aeronomy* (Academic Press, Inc., New York and London).

BAXTER, R.G. (1967): A numerical solution of the time-varying diffusion equation for the F_2-layer, *Planet. Space Sci.*, **15**, 701-713.

BILITZA, D., K. RAWER, L. BOSSY and T. GULYAEVA (1993): International reference ionosphere-past, present and future: II. Plasma temperatures, ion composition and ion drift, *Adv. Space Res.*, **13** (3), (3)15-(3)23.

CHANDLER, M.O. and C.R. CHAPPELL (1986): Observations of the flow of H^+ and He^+ along magnetic field lines in the plasmasphere, *J. Geophys. Res.*, **91**, 8847-8860.

DAHLQUIST, G. and A. BJÖRCK (1974): *Numerical Methods* (Prentice Hall, Inc., Englewood Cliffs, N.J.).

DUDENEY, J.R. (1983): The accuracy of simple methods for determining the height of the maximum electron concentration of the F_2-layer from scaled ionospheric characteristics, *J. Atmos. Terr. Phys.*, **45**, 629-640.

FÖRSTER, M. and N. JAKOWSKI (1988): The Nighttime Winter Anomaly (NWA) effect in the American sector as consequence of interhemispheric ionospheric coupling, *Pure Appl. Geophys.*, **127**, 447-471

GEAR, C.W. (1971): *Numerical Initial Value Problems in Ordinary Differential Equations* (Prentice Hall, Inc., Englewood Cliffs, N.J.).

HAGAN, M.A., J.M. FORBES and M. CODRESCU (1990): A numerical investigation of thermosphere-ionosphere interaction over Millstone Hill, *Planet. Space Sci.*, **38**, 1541-1549.

HARGREAVES, J.K. (1992): *The Solar-Terrestrial Environment* (University Press, Cambridge, England).

HEDIN, A.E. (1991): Extension of the MSIS thermosphere model into the middle and lower atmosphere, *J. Geophys. Res.*, **96** (A2), 1159-1172.

HEDIN, A.E., M.A. BIONDI, R.G. BURNSIDE, G. HERNANDES, R.M. JOHNSON, T.L. KILEEN, C. MAZAUDIER, J.W. MERIWETHER, J.E. SALAH, R.J. SICA, R.W. SMITH, N.W. SPENCER, W.B. WICKWAR and T.S. VIRDI (1991): Revised global model of thermosphere winds using satellite and ground-based observations. *J. Geophys. Res.*, **96**, 7657-7688.

KENDALL, P.C. (1962): Geomagnetic control of diffusion in the F_2-region of the ionosphere. I) The form of the diffusion operator, *J. Atmos. Terr. Phys.*, **24**, 805-811.

KOLEVA, R. and I. KUTIEV (1987): Effect of the electrodynamic drift on a steady-state model of the low-latitude ionosphere, *Compt. R. Acad. Bulg. Sci.*, **40** (8), 53-55.

KOLEVA, R. and I. KUTIEV (1990): Variations of helium ion density from theoretical considerations, *Adv. Space Res.*, **10** (8), (8)95-(8)98.

KUTIEV, I. (1986): Structure and dynamics of the topside ionosphere, *D. Sc. Thesis*, Bulgarian Academy of Sciences, Sofia.

KUTIEV, I.S. and S.M. STANKOV (1994): Relative abundance of H^+ and He^+ in outer ionosphere, *Adv. Space Res.*, **14** (12), (12)139-(12)141

KUTIEV, I.S. and S.M. STANKOV (1995): Review of progress in gathering, distributing, and using satellite data for activities within PRIME, in: *Proceedings of the COST 238/PRIME Workshop, 5-6 September 1994, El Arenosillo-Huelva, Spain, «Developing and Testing of an Electron Density Height Profile Model for PRIME»*, 281-287.

KUTIEV, I.S., S.M. STANKOV and P. MARINOV (1994): Analytical expression of O^+-H^+ transition surface for use in IRI, *Adv. Space Res.*, **14** (12), (12)135-(12)138.

LINDZEN, R.S. (1966): Crude estimate for the zonal velocity associated with the diurnal temperature oscillation in the thermosphere, *J. Geophys. Res.*, **71** (3), 865-870.

MOFFETT, R.J. and J.A. MURPHY (1973): Coupling between the *F*-region and protonosphere: numerical solution of the time-dependent equations, *Planet. Space Sci.*, **21**, 43-52.

MURPHY, J.A. and R.J. MOFFETT (1978): Induced proton flow in a collapsing post-sunset ionosphere and protonosphere, *Planet. Space Sci.*, **26**, 281-288.

MURPHY, J.A. and A.A. NAGHMOOSH (1979): A theoretical study of downward H^+ field-aligned velocities at mid-latitudes, *Planet. Space Sci.*, **27**, 297-302.

MURPHY, J.A., G.J. BAILEY and R.J. MOFFETT (1980): A theoretical study of the effects of quiet-time electromagnetic drifts on the behaviour of thermal plasma at mid-latitudes, *J. Geophys. Res.*, **85** (A5), 1979-1986.

NAGHMOOSH, A.A. and J.A. MURPHY (1983): A comparative study of H^+ and He^+ at sunspot minimum and sunspot maximum, *J. Atmos. Terr. Phys.*, **45** (10), 673-682.

NAMGALADZE, A.A., YU. N. KORENKOV, V.V. KLIMENKO, I.V. KARPOV, F.C. BESSARAB, V.A. SUROTKIN, T.A. GLUSHCHENKO and N.M. NAUMOVA (1990): A global numerical model of the Earth's thermosphere, ionosphere, and protonosphere, *Geomagn. Aeron.*, **30** (4), 515-521.

RAITT, W.J., R.W. SCHUNK and P.M. BANKS (1978): Helium ion outflow from the terrestrial ionosphere, *Planet. Space Sci.*, **26** (3), 535-557.

RICHARDS, P.G. and D.G. TORR (1985): Seasonal, diurnal, and solar cyclical variations of the limiting H^+ flux in the Earth's topside ionosphere, *J. Geophys. Res.*, **90** (A6), 5261-5268.

RISHBETH, H. (1985): On the F_2-layer continuity equation, *J. Atmos. Terr. Phys.*, **48** (6), 511-519.

RISHBETH, H. and R. EDWARDS (1989): The isobaric F_2-layer, *J. Atmos. Terr. Phys.*, **51** (4), 321-338.

RISHBETH, H. and O.K. GARRIOTT (1969): *Introduction to Ionospheric Physics* (Academic Press, Inc., New York and London).

RISHBETH, H., S. GANGULY and J.C.G. WALKER (1978): Field-aligned and field-perpendicular velocities in the ionospheric F_2-layer, *J. Atmos. Terr. Phys.*, **40**, 767-784.

ROBLE, R.J., E.C. RIDLEY and A.D. RICHMOND (1988): A coupled thermosphere/ionosphere general circulation model, *Geophys. Res. Lett.*, **15**, 1325-1328.

SCHUNK, R.W. and J.C.G. WALKER (1969): Thermal diffusion in the topside ionosphere for mixtures which include multiply-charged ions, *Planet. Space Sci.*, **17** (5), 853-868.

SCHUNK, R.W. and J.C.G. WALKER (1970): Thermal diffusion in the F_2-region of the ionosphere, *Planet. Space Sci.*, **18** (4), 535-557.

SICA, R.J., R.W. SCHUNK and P.J. WILKINSON (1990): A study of the undisturbed mid-latitude ionosphere using simultaneous multiple site ionosonde measurements during the Sundial-86 campaign, *J. Geophys. Res.*, **95** (A6), 8271-8279.

STANKOV, S.M. (1990): A new coordinate change in mathematical modelling of the upper ionosphere, *Compt. R. Acad. Bulg. Sci.*, **43** (11), 39-41.

STERLING, D.L., W.B. HANSON, R.J. MOFFETT and R.G. BAXTER (1969): Influence of electromagnetic drifts and neutral air winds on some features of the F_2-region, *Radio Sci.*, **4**, 1005-1023.

STROBEL, D. F. and M.B. MCELROY (1970): The F_2-layer at middle latitudes, *Planet. Space Sci.*, **18**, 1181-1202.

STUBBE, P. (1970): Simultaneous solution of the time dependent coupled continuity equations, heat conduction equations, and equations of motion for a system consisting of a neutral gas, an electron gas, and a four component ion gas, *J. Atmos. Terr. Phys.*, **32**, 865-903.

STUBBE, P. (1973): *The Thermosphere and the F-Region: a Reconciliation of Theory with Observations*, Ionosphere Research Laboratory, Pennsylvania State University, Scientific Report No. 418.

SZUSZCZEWICZ, E.P., B. FEJER, E. ROELOF, R. SCHUNK, R. WOLF, R. LEITINGER, M. ABDU, B.M. REDDY, J. JOSELYN, P. WILKINSON and R. WOODMAN (1988): SUNDIAL: a world-wide study of interactive ionospheric processes and their roles in the transfer of energy and mass in the Sun-Earth system, *Annales Geophysicae*, **6**, 3-18.

TOBISHKA, W.K. and C.A. BARTH (1990): A solar EUV flux model, *J. Geophys. Res.*, **95** (A6), 8243-8251.

WALDMAN, H. (1973): The specification of distributed boundary conditions in numerical simulation of the ionosphere, *J. Atmos. Terr. Phys.*, **35**, 2205-2215.

YOUNG, E.R., D.G. TORR, P.G. RICHARDS and A.F. NAGY (1980): A computer simulation of the mid-latitude plasmasphere and ionosphere, *Planet. Space Sci.*, **28** (8), 881-893.

(received January 12, 1996;
accepted May 9, 1996)